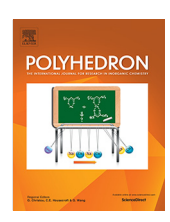


Contents lists available at ScienceDirect

# Polyhedron

journal homepage: www.elsevier.com/locate/poly



# Synthesis, crystallography, spectroscopy, and kinetics involving the fluorimetric detection of metal ions by internal imine derivatives of anthraquinone-18-crown-5 in aqueous media



Anwar Hussain, Luke Lewandowski, Dawson C. Cork, Kadarkaraisamy Mariappan, Andrew G. Sykes\*

Contribution from the Department of Chemistry, University of South Dakota, Vermillion, SD 57069, United States

#### ARTICLE INFO

Article history: Received 26 December 2020 Accepted 19 February 2021 Available online 4 March 2021

Keywords:
Anthraquinone
Crown ethers
Luminescent sensors
Kinetics
Crystallography

#### ABSTRACT

We have selectively synthesized and characterized several aliphatic internal imine isomers which show selectivity towards various transition metal ions with large shifts in the UV–Vis and OFF–ON switching of fluorescence in solution. The stoichiometry with different transition metals has been determined to be 1:1, with the 1,2-ethlenediamine dimer showing the best selectivity towards Hg(II). Selectivity in different solvent media and the varying kinetics of transition metal binding with the macrocycle has been presented along with the crystallography of the ligands and their metal complexes.

© 2021 Elsevier Ltd. All rights reserved.

#### 1. Introduction

Exposure to heavy metals is dangerous to human health [1], and the detection of heavy metals often require time (i.e. electroanalysis [2]) and expensive equipment (ICP-MS [3]). Due to their high selectivity and sensitivity, fluorescent chemosensors have been widely used in various fields, including environmental science, pharmacology, biology, and physiology [3]. Typically, fluorescent chemosensors are molecules that are capable of binding the analyte of interest selectively and reversibly with a concomitant change in absorption and/or fluorescent spectra. Various fluorescent chemosensors for biologically or/and environmentally essential cations [4], anions [5], neutral molecules [6], and biomolecules [7] have been developed in which detection is based on a variety of photophysical mechanisms, such as photoinduced electron transfer (PET), photoinduced charge transfer (PCT), fluorescence resonance energy transfer (FRET), excimer-exciplex formation, and tautomerization [8], with the number of mechanisms slowly expanding [9,10].

In this regard, our group is actively working with macrocyclic ligands based on an anthraquinone platform similar to compound **1**. The anthraquinone moiety acts as a fluorophore, providing different selectivity for different cations, depending upon the Lewis bases present within the macrocyclic ring [11,12]. The internal carbonyl group of the anthraquinone co-ordinates to the cation and

causes structural rigidification, and undergoes internal charge transfer, leading to different emission wavelengths. These molecules contain a low-lying  $n-\pi^*$  transition and do not luminescence; however, coordination of the cation raises the energy of  $n-\pi^*$  transition above the emissive  $\pi-\pi^*$  transition, switching the fluorescence from OFF to ON [11]. We have previously shown that compound 1 selectively detects Pb(II) ion in a solution [11], and we have also reported the synthesis and characterization of imines formed with the external carbonyl group using aromatic amines and TiCl<sub>4</sub> as a catalyst (Scheme 1) [13]. Here, because the imine is external to the ring, selectivity did not change appreciably from 1, suggesting that the intra-annular Lewis base is responsible for selectivity and sensitivity of metal-ion recognition in theses system. Hence, modifying the internal carbonyl to make internal imines will potentially influence selectivity to a greater degree.

In this paper, we report the synthesis of internal imine-based chemosensors for the detection of transition metal ions with large shifts in the ground state UV-Vis spectra and OFF-ON switching of fluorescence in solution. The selectivity of the imine-based chemosensors in different solvent media is presented along with the stoichiometric and kinetic studies with different transition metals and the crystallography of the ligands.

## 2. Experimental methods

All reagents and solvents were purchased from commercially available vendors and used without any further purification unless it is mentioned. Tetrahydrofuran (THF) was dried by using the pre-

<sup>\*</sup> Corresponding author. E-mail address: Andrew.Sykes@usd.edu (A.G. Sykes).

Scheme 1. Internal vs. external imines derived from the anthraquinone macrocycle in center (1).

vious method found in the literature [14]. Nuclear Magnetic Resonance (NMR) spectra were collected in CDCl<sub>3</sub> on a Bruker Ascend™ 400 MHz at the room temperature and the chemical shifts were reported in part per million (ppm). Fourier Transform-Infra Red spectroscopy (FT-IR) spectra were collected on Bruker Alpha FT-IR spectrometer and the wavenumber is reported in cm<sup>-1</sup>. Element analyses were carried out by using Exeter Analytic Instrument model number CE-440 and Helium gas was used as the carrier gas. UV-Vis and luminescence spectra were collected by using Varian Cary 50 Bio UV-Vis spectrometer and FluoroMax-4 respectively. The stoichiometric and rate constant of the metal-complex formation were determined by using UV-Vis spectra via Job's plot and curve-fitting models. Electrospray Ionization-Mass spectroscopy (ESI-MS) of the samples were collected in Varian 500-MS Ion Trap Mass spectrometer by using a very diluted acetonitrile solution of samples. Crystallographic data were recorded on Bruker CCD Apex II diffractometer and Bruker D8 Venture at 100 K using  $MoK_{\alpha}$  radiation. The crystallographic data were integrated by Apex II and Apex III software and the structures were solved by using SIR97 [15], SHELXT [16] and refined with SHELXL [17] followed by further refinement and completion of the structure on WinGX [18] and Mercury 4.3.1 is used to visualize the structures. The graphical spectra were plotted by using OriginPro 9.0 software. The reaction schemes and chemical structures were drawn on BIO-VIA Draw for academic use by Dassault Systèmes.

# 3. Results and discussion

Internal imine derivatives 2-5 were synthesized by adding aniline (1 equivalent), primary amines (excess), and acetic acid to a stirred solution of 1 [16] (0.25 mmol) in absolute ethanol or methanol (Scheme 2). The synthetic procedure and characterization data of the precipitated solids are provided in the supporting material (<sup>1</sup>H NMR, elemental analyses, ESI-MS, FT-IR spectroscopy, and single-crystal X-ray diffraction). Whereas Compound 1 is symmetrical through the central carbonyl groups, compounds 2-4 are asymmetric due to the imine group, and hence the NMR spectra show six aromatic protons (Figs. S6-S8) instead of three. The proton peaks of the polyether groups are also mixed with the proton peaks of the alkyl groups of the primary amine: however, the integrated ratios indicate the total number of alkyl and polyether peaks are as expected. The formation of the imine bond is characterized by FT-IR spectroscopy with the appearance of new sharp peaks between 1630 and 1615 cm<sup>-1</sup> (absent in 1), shown in Fig. S14, due to the C=N stretching generally present in Schiff bases previously reported between 1650 and 1608 cm<sup>-1</sup> [19]. The imine derivatives were further characterized by elemental analyses, ESI-

MS (Figs. S10-S13), and single-crystal X-ray crystallography (Figs. S29-S32) and are included in the supporting material. At this time, we have been unable to extend the synthesis to the formation of aromatic imines, instead isolating simple 1:1 hydrogen-bonded adducts of compound 1 and any aromatic amine starting material, potentially because of the reduced basicity of the aromatic amine.

# 3.1. UV-Vis and fluorescence response

The optical properties of compounds **2–5** in response to added metal ions were studied by the addition of two equivalents of different metal salts with the host macrocycle and the resulting UV–Vis and fluorescence spectra recorded. All the cations were dissolved in dry acetonitrile except K(I), Rb(I), and Cs(I) perchlorate salts which were dissolved in H<sub>2</sub>O, due to poor solubility in acetonitrile. The UV–Vis spectra of compounds **2–4** in acetonitrile and compound **5** in CH<sub>2</sub>Cl<sub>2</sub>:CH<sub>3</sub>OH (9:1) with added cations result in large bathochromic shifts of  $\lambda_{max}$  (Compound **3** (Fig. 1A), Compound **2–5** Figs. S15–S18). The corresponding increases in fluorescence response are provided in Fig. 1B and S21–S24. The internal quantum yield of **3** with perchlorate salts of Zn(II) were measured in CH<sub>3</sub>CN and found to be lower ( $\Phi$  = 0.45%) as compared to the perchlorate complex of **1** and H<sub>3</sub>O<sup>+</sup> ( $\Phi$  = 1.4%), Ca(II) ( $\Phi$  = 1.6%), and Pb(II) ( $\Phi$  = 2.2%) [11].

The collective fluorescence responses of compounds **2–4** is shown in Fig. 2A, showing that most alkali and alkali earth metals, with the exception of Mg(II) ion, do not change the fluorescence (or absorbances respectively)  $\lambda_{max}$  of these compounds; however, most of the transition metals that were tested do cause a significant change in absorbance and large OFF-ON increases in fluorescence intensity. In addition, NH<sub>4</sub> and H<sup>+</sup> also show luminescence turn-on with compounds 2-3, and all three compounds exhibit the same collective pattern response, with some minor changes in overall fluorescence intensity due to minor variations in either concentration or instrument setup. In Fig. 2B, compound 3 was tested against the same battery of cations in different solvent systems - acetonitrile (blue), 10% water:acetonitrile (orange); 10% HEPES buffer: acetonitrile (gray); raw data for the different solvent systems can be found in Figs. S22, S25 & S26. Again there are no significant differences in the pattern of intensities between the different solvent system, with the exception of Mg(II) and Mn(II) which has a significant enhancement in acetonitrile, but not when in the presence of water, most likely due to the high hydration energy of these cations. However, compound 5 was found to be more selective toward the Hg(II) as shown in Figs. S18 & S24.

Scheme 2. Schematic representation of the preparation of imine-derivatives.

#### 3.2. Stoichiometric studies & kinetics

Stoichiometric titration studies were carried out for compound **3** with three different metal perchlorate salts of Zn(II), Mg(II), and Mn(II) as shown in Fig. 3. The stoichiometry of Zn(II), Mg(II), or Mn (II) were all determined to be 1:1 as they all saturate with one equivalent of the added cation which is also verified by Job's plot showing maximum  $\sim$ 0.5 at ratio of [M<sup>n+</sup>]/([3]+[M<sup>n+</sup>]) (Figs. S35-S37). All cation additions show large bathochromic shifts(from 350 nm to 400 nm) with clean isosbestic points at  $\sim$ 365 nm for each addition.

Due to poor stoichiometric results initially with Mg(II) and Mn (II), extra time was added between successive aliquot additions in order for the encapsulation of the metal cation to be complete. Complete kinetic studies were also carried out at room temperature for compound 3 with 2.0 equivalent of added Zn(II), Mg(II), and Mn(II), and the UV–Vis spectrum recorded with 10-s intervals as shown in Fig. 4. The kinetic studies indicated the maximum intensity for UV–Vis at 400 nm occurs instantaneously for Zn(II) (Fig. S27) and doesn't change throughout the scans; however, the formation of maximum intensity at 400 nm for Mg(II) and Mn(II) is delayed (Fig. 4 for Mn(II) and Fig. S28 for Mg(II)), which is apparently due to the loss of water molecules around the hydrated cations as shown in Eq. (1) before making a complex with the host macrocycle.

$$M(H_2O)_x^{m+} \rightleftharpoons M(H_2O)_{x-n}^{m+} + nH_2O$$
 (1)

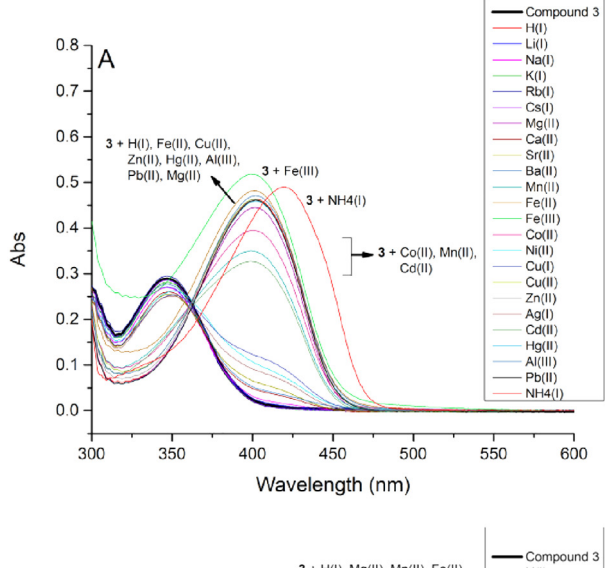
Subsequently,  $\ln(A_f-A_i)$  plotted against time in s for Mg(II) and Mn(II) resulted in a linear fit indicating first-order kinetics for complex formation with **3**. The rate constants for Mg and Mn addition were 0.0089 s<sup>-1</sup> (t<sub>1/2</sub> = 77.88 s), and 0.0062 s<sup>-1</sup> (t<sub>1/2</sub> = 110.73 s) respectively. These results parallel the general lability of these cations.

# 3.3. Single crystal X-ray crystallography (SC-XRD)

X-ray quality single crystals of compounds **2–5** were grown by solvent diffusion techniques. The crystallography data for all compounds are given in Table 1 and the thermal ellipsoid diagram are given in Figs. S29-S33. The X-ray crystal structure data for the imine bond and geometry is provided in Table 2.

The imine bond (C9=N1) has a length equal to 1.28 Å, which is comparable to the C=N bond length (1.27 Å) [20] confirming the formation of the carbon–nitrogen double bond. The carbon–nitrogen single bond (C23-N1) has a length equal to 1.45 Å which is comparable with C–N (1.47 Å) [20]. The geometry at C10 is trigonal planar and the carbonyl bond length (C10=O1) is 1.22 Å and the bond angles C11—C10—O1 or C14—C10—O1 is 120° to 121° which is comparable to the bond length and angle of the carbonyl group. The geometry at C9 is distorted from perfect trigonal planar with the bond angle of C12—C9—N1 or C13—C9—N1 ranges from 115° to 128° suggesting that the internal carbonyl group has been converted into imines.

We have been unsuccessful in growing single crystals that contain an encapsulated metal ion within these new macrocycles. Our



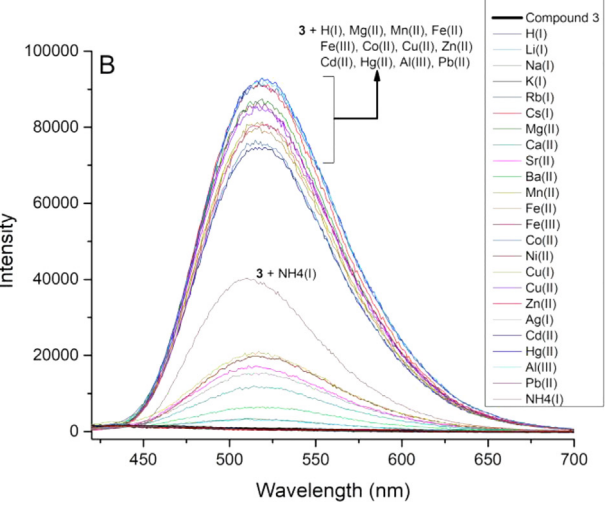


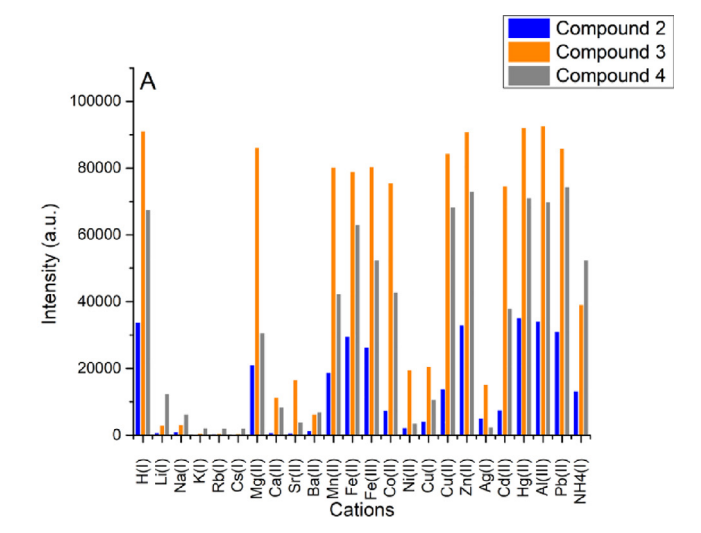
**Fig. 1.** A. UV–Vis spectra of compound **3** ( $5.0 \times 10^{-5}$  M) in CH<sub>3</sub>CN before (black) and after addition of 2.0 equivalents of cations as perchlorate salts. B. Emission spectra of compound **3** ( $5.0 \times 10^{-5}$  M) in CH<sub>3</sub>CN before and after the addition of 2.0 equivalents of cations ( $\lambda_{\text{ext}} = 365$  nm).

attempts to grow crystals of compound **3** with Mn(II) or Mg(II) yielded only the protonated ligand [**3**.H $^+$ ]ClO<sub>4</sub> (Fig. S31) with a perchlorate counter-ion. Two molecules are present in the asymmetric unit, with both of the imine nitrogen atoms protonated. Over a long period of time (i.e. growing crystals by evaporation or vapor diffusion), through the introduction of atmospheric water, these acidic cations produce sufficient acid (Equation (2)) to form crystals of [**3**.H $^+$ ](ClO<sub>4</sub>).

$$M(H_2O)_x^{2+} + H_2O \rightleftharpoons M(H_2O)_{x-1}(OH)^{1+} + H_3O^+$$
 (2)

Our attempts to grow X-ray quality crystals of compound **3** with Zn(II) in acetonitrile/ether mixtures did give pale yellow crystals; however the crystal structure does not show Zn(II) bound inside the macrocyclic cavity, rather the imine functionality has been hydrolyzed back to the anthraquinone starting material, indicating that over long periods (typically several days), these imine compounds are unstable (Fig. S34). The crystal structure of **1** with Zn(II) is isostructural to what has been reported previously and has a better final *R* indices, i.e. 0.055 vs. the already reported value of 0.067 [111].

An additional goal was to synthesize internal imines using aromatic amines such as aniline and *p*-nitroaniline with **1**, however,



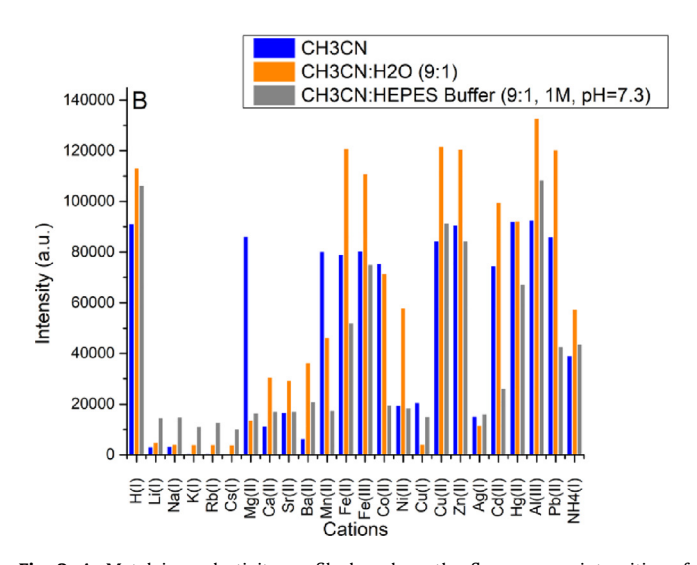
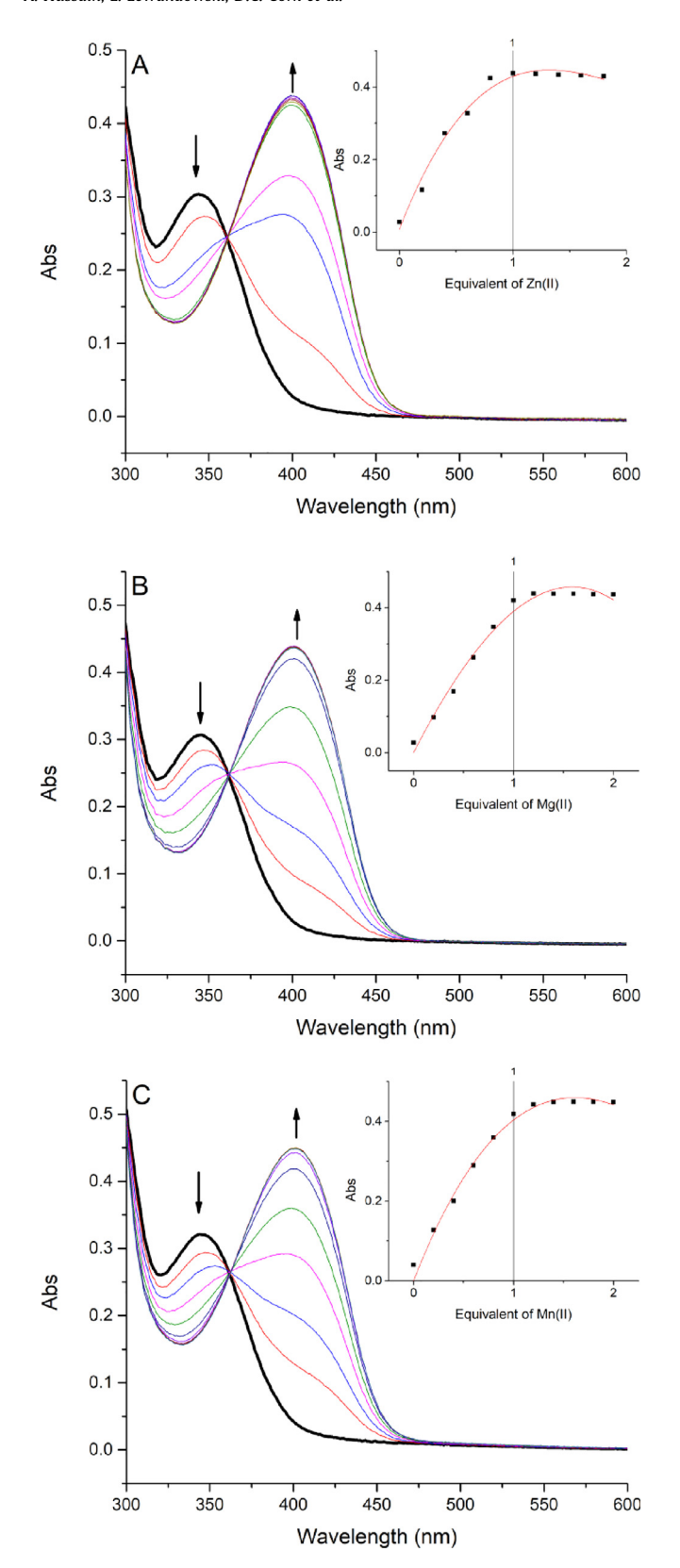


**Fig. 2.** A. Metal ion selectivity profile based on the fluorescence intensities of compound **2–4** in CH<sub>3</sub>CN at 520 nm. B. Metal ion selectivity profile based on the fluorescence intensities of compound **3** in the different solvent systems (acetonitrile - blue; 10% H<sub>2</sub>O:CH<sub>3</sub>CN - orange, and 10% HEPES buffer:CH<sub>3</sub>CN - gray) at 520 nm.

the only products isolated showed simple adduct formation with the formation of a hydrogen bond between the amine and the internal carbonyl (shown in Fig. 5 with p-nitroaniline and Fig. S33 with aniline). The N–H…O = hydrogen bond measures  $\sim 2.94$  Å, a slightly long hydrogen bond distance of an unprotonated amine.

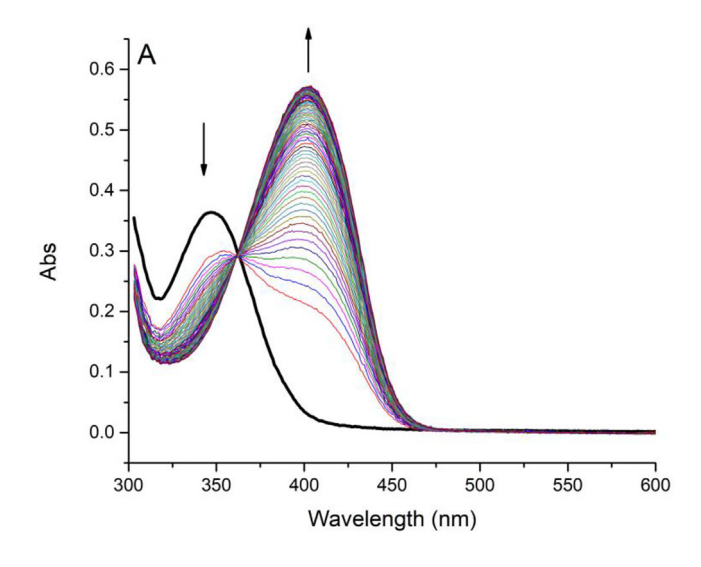
#### 4. Conclusions

In summary, various internal imine derivatives of 1,8-anthraquinone-18- crown-5 were selectively synthesized in the presence of aniline and acetic acid. Internal imine derivatives were highly sensitive towards various cations with large bathochromic shifts in the UV-Vis and OFF-ON switching of fluorescence in different solvent systems. Imine derivatives had the same general cation selectivity and ruled out that enhanced fluorescence is due to protonation by using a buffered solution. Stoichiometric studies with different transition metals indicated the formation of 1:1 host:cation adducts; however, over long periods of time, either protonation or hydrolysis of the imine is observed with different metal cations. This work also shows that the basicity of the imine nitro-



**Fig. 3.** UV–Vis titration of  $5.0\times10^{-5}$  M of compound **3** in CH<sub>3</sub>CN with an increasing amount of M(II) perchlorate salts added. Insets – plots of intensity vs equivalents M (II) monitored at 400 nm. A. Zn(II), ~30 s between scans; B. Mg(II), ~4 min between scans; and C. Mn(II), ~3 min between scans.

gen plays a large role in controlling the selectivity of this macrocycle. We are still attempting to synthesize substituted aromatic amines that would allow us to better tune the basicity of the host



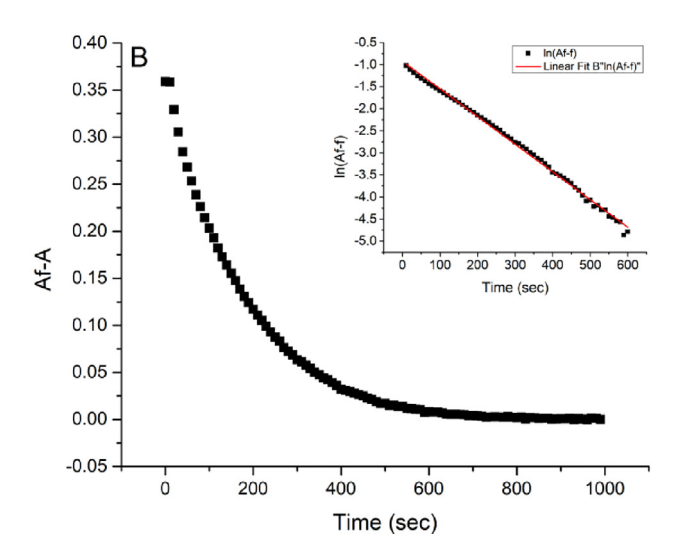


**Fig. 4.** A. Kinetic spectra of compound **3** (5.0  $\times$  10<sup>-5</sup> M) with 2 equivalents added Mn(II) in CH<sub>3</sub>CN taken every 10 sec for 100 scans. B. Absorbance (A<sub>I</sub>-A<sub>i</sub>) vs time monitored at 400 nm and inset showing the linear fit of  $\ln(A_I-A_i)$  vs time indicating the first-order kinetic process with the rate constant 0.0062 s<sup>-1</sup> (t<sub>1/2</sub> = 110 s).

macrocycle to improve the selectivity and solubility, in our search for cost-efficient and environment-friendly chemosensors for the detection of a wide range of heavy metal cations.

## **Declaration of Competing Interest**

The authors declare that they have no known competing financial interests or personal relationships that could have appeared to influence the work reported in this paper.

#### Acknowledgment

The authors would like to thank the Center for Fluorinated Functional Materials (CFFM) for financial support, NSF-MRI-CHE-1919637 for the purchase of a Bruker Dual-Source Single-Crystal X-ray Diffractometer, and Mr. Clinton Bruce Gray, Department of Chemistry, the University of South Dakota for elemental analyses and ESI-MS results. L. Lewandowski thanks NSF-REU-1757652 for financial support.

**Table 1**Crystallographic data table for CEN-derivatives for compound 2–5 showing important parameters such as unit cell, crystal system, space group, etc.

	compound 2	[3H] <sup>+</sup> ClO <sub>4</sub> .ACN	compound 4	compound 5	[1.p-nitroaniline]	[1.aniline].CH <sub>2</sub> Cl <sub>2</sub>
Empirical Formula	C <sub>24</sub> H <sub>27</sub> NO <sub>7</sub>	C48H55Cl2N3O20	C <sub>24</sub> H <sub>27</sub> NO <sub>6</sub>	$C_{46}H_{48}N_2O_{12}$	$C_{28}H_{28}N_2O_9$	C <sub>26</sub> H <sub>26</sub> Cl <sub>2</sub> NO <sub>7</sub>
Formula Weight	441.46	1064.85	425.46	820.88	536.52	535.38
Temperature (K)	100	100	100	100	100	100
Crystal System	monoclinic	triclinic	monoclinic	monoclinic	monoclinic	monoclinic
Space Group	C 2/c	P-1	C 2/c	P121/c1	C12/c1	C12/c1
Unit Cell (Å, °)	a = 23.978(3)	a = 8.7079(12)	a = 24.575(7)	a = 8.1704(18)	a = 20.3136(32)	a = 26.9992(7)
	b = 8.5013(11)	b = 11.4703(16)	b = 8.096(2)	b = 22.6799(50)	b = 12.3436(19)	b = 12.3643(3)
	c = 23.789(5)	c = 24.868(3)	c = 24.078(10)	c = 21.7773(50)	c = 21.7545(34)	c = 15.0280(4)
	$\alpha = 90$	$\alpha = 80.711(2)$	$\alpha = 90$	$\alpha = 90$	$\alpha = 90$	$\alpha = 90$
	$\beta = 119.102(2)$	$\beta$ = 87.626(2)	$\beta = 117.668(3)$	$\beta = 91.610(7)$	$\beta = 105.737(2)$	$\beta = 91.910(1)$
	$\gamma = 90$	$\gamma = 77.303(2)$	$\gamma = 90$	$\gamma = 90$	$\gamma = 90$	$\gamma = 90$
Volume (Å <sup>3</sup> )	4237.1(11)	2391.3(6)	4243(2)	4033.82(18)	5250.32(34)	4013.95(3)
Z	8	2	8	4	4	8
Density Diffraction	1.384	1.479	1.332	1.38	1.36	1.41
Absorption coefficient	0.096	0.222	0.096	0.101	0.102	0.306
F(000)	1872	1116	1808	1776	2256	2248
θ Range	1.96-27.62	0.83-27.93	1.96-25.48	2-25.4	1.9-28.9	2.2-34.3
Index Ranges	±31 ± 11 ± 30	±11 ± 15 ± 32	±29 ± 9 ± 29	±9 ± 27 ± 26	±27 ± 16 ± 29	±42 ± 19 ± 23
Reflection collected	24,776	29,249	21,190	56,762	31,657	51,888
Independent reflections	4897	11,214	3935	7386	6550	8886
Observed reflections	2707	7928	2395	3249	4780	7745
Goodness-of-fit (GOOF)	0.953	1.063	1.028	1.006	1.041	1.092
Final R indices $[I > 2\sigma(I)]$	0.0587	0.0527	0.0524	0.073	0.045	0.046
R indices (all data)	0.1263	0.0806	0.1020	0.1940	0.070	0.053
CCDC deposit number	2050184	2050189	2050188	2050177	2050187	2050181

 Table 2

 Important bond lengths and angles of different connectivity in the crystal structure of different compounds including the distance between imine nitrogen and polyether oxygen atoms.

	compound 2	[3H] <sup>+</sup> ClO <sub>4</sub> .ACN	compound 4	compound 5
Bond Lengths				
C10-O1	1.223	1.229	1.226	1.229
C9-N1	1.284	1.298	1.281	1.284
N1-C23	1.454	1.459	1.455	1.454
Bond Angles				
C12-C9-N1	115.36	118.82	128.98	128.19
C13-C9-N1	127.89	123.03	115.55	117.27
C11-C10-O1	121.06	121.01	121.05	121.41
C14-C10-O1	121.4	121.45	121.59	121.76
C9-N1-C23	123.83	128.34	123.17	120.49
Distance between imine	nitrogen and polyether oxygen atoms	5		
N1-06	4.834	3.713	4.645	4.169
N1-05	3.955	4.049	4.198	4.421
N1-04	4.308	3.051	3.937	4.379

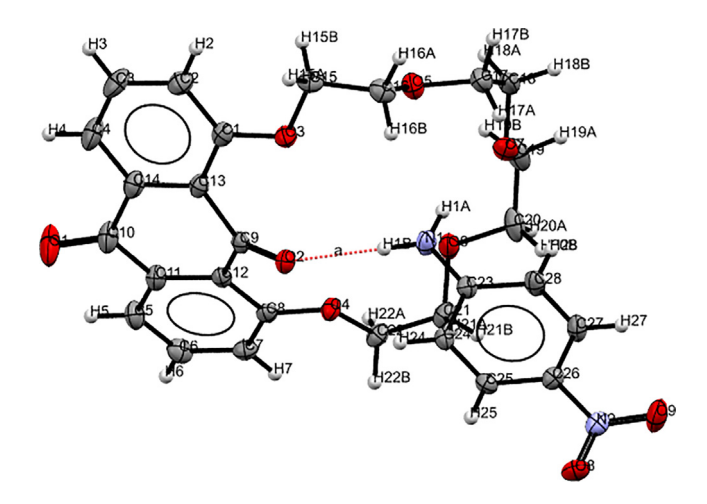


**Fig. 5.** Thermal ellipsoid diagram (50%) of compound **1** with p-nitroaniline showing carbon (grey), oxygen (red), nitrogen (purple), and hydrogen (white) and indicating hydrogen-bond between **1** and p-nitroaniline.

# Appendix A. Supplementary data

CCDC 2050184, CCDC 2020189, CCDC 2050188, CCDC 2050177, CCDC 2050187, CCDC 2050181 contains the supplementary crystallography data for compound **2**, [3H]\*ClO4.ACN, **4**, **5**, [1.p-nitroaniline], [1.aniline].CH2Cl2 respectively. These data can be obtained free of charge via https://www.ccdc.cam.ac.uk/structures/, or from the Cambridge Crystallographic Data Centre, 12 Union Road, Cambridge CB2 1EZ, UK; fax: (+44) 1223-336-033; or email: deposit@ccdc.cam.ac.uk. Supplementary data to this article can be found online at https://doi.org/10.1016/j.poly.2021. 115120.

#### References

- [1] S. Martin, W. Griswold, Human health effects of heavy metals, Environmental Science and Technology briefs for citizens 15 (2009) 1–6.
- [2] B. Bansod, T. Kumar, R. Thakur, S. Rana, I. Singh, A review on various electrochemical techniques for heavy metal ions detection with different sensing platforms, Biosens. Bioelectron. 94 (2017) 443–455.
- [3] D. Wu, A.C. Sedgwick, T. Gunnlaugsson, E.U. Akkaya, J. Yoon, T.D. James, Fluorescent chemosensors: the past, present and future, Chem. Soc. Rev. 46 (23) (2017) 7105–7123.

- [4] Y.-D. Cao, Q.-Y. Zheng, C.-F. Chen, Z.-T. Huang, A new fluorescent chemosensor for transition metal cations and on/off molecular switch controlled by pH, Tetrahedron Lett. 44 (25) (2003) 4751–4755.
- [5] V. Thiagarajan, P. Ramamurthy, D. Thirumalai, V.T. Ramakrishnan, A novel colorimetric and fluorescent chemosensor for anions involving PET and ICT pathways, Org. Lett. 7 (4) (2005) 657–660.
- [6] F.P. Cossío, A. Arrieta, V.L. Cebolla, L. Membrado, J. Vela, R. Garriga, M.P. Domingo, Berberine cation: A fluorescent chemosensor for alkanes and other low-polarity compounds. An explanation of this phenomenon, Org. Lett. 2 (15) (2000) 2311–2313.
- [7] N. Soh, T. Ueda, Perylene bisimide as a versatile fluorescent tool for environmental and biological analysis: A review, Talanta 85 (3) (2011) 1233–1237.
- [8] P.N. Basa, A.G. Sykes, Differential sensing of Zn (II) and Cu (II) via two independent mechanisms, J. Org. Chem. 77 (19) (2012) 8428–8434.
- [9] A. Barba-Bon, A.M. Costero, S. Gil, M. Parra, J. Soto, R. Martínez-Máñez, F. Sancenón, A new selective fluorogenic probe for trivalent cations, Chem. Commun. 48 (24) (2012) 3000–3002.
- [10] B. Kaur, N. Kaur, S. Kumar, Colorimetric metal ion sensors—a comprehensive review of the years 2011–2016, Coord. Chem. Rev. 358 (2018) 13–69.
- [11] M. Kadarkaraisamy, A.G. Sykes, Luminescence detection of transition and heavy metals by inversion of excited states: synthesis, spectroscopy, and X-ray crystallography of Ca, Mn, Pb, and Zn complexes of 1, 8-anthraquinone-18crown-5, Inorg. Chem. 45 (2) (2006) 779–786.

- [12] M. Kadarkaraisamy, A.G. Sykes, Selective luminescence detection of cadmium (II) and mercury (II) utilizing sulfur-containing anthraquinone macrocycles (part 2) and formation of an unusual Hg22+-crown ether dimer via reduction of Hg (II) by DMF, Polyhedron 26 (6) (2007) 1323–1330.
- [13] P.N. Basa, A. Bhowmick, M.M. Schulz, A.G. Sykes, Site-selective imination of an anthracenone sensor: selective fluorescence detection of barium (II), J. Org. Chem. 76 (19) (2011) 7866–7871.
- [14] A. Schwartz, The benzophenone/ketyl tetrahydrofuran (THF) still, Chem. Eng. News 56 (1978) 88.
- [15] A. Altomare, M.C. Burla, M. Camalli, G.L. Cascarano, C. Giacovazzo, A. Guagliardi, A.G. Moliterni, G. Polidori, R. Spagna, SIR97: a new tool for crystal structure determination and refinement, J. Appl. Crystallogr. 32 (1) (1999) 115–119.
- [16] G.M. Sheldrick, SHELXT-Integrated space-group and crystal-structure determination, Acta Crystallogr. Sect. A: Found. Adv. 71 (1) (2015) 3–8.
- [17] G.M. Sheldrick, Crystal structure refinement with SHELXL, Acta Crystallogr. Sect. C: Struct. Chem. 71 (1) (2015) 3–8.
- [18] L.J. Farrugia, WinGX suite for small-molecule single-crystal crystallography, J. Appl. Crystallogr. 32 (4) (1999) 837–838.
- [19] R. Parashar, R. Sharma, A. Kumar, G. Mohan, Stability studies in relation to IR data of some Schiff base complexes of transition metals and their biological and pharmacological studies, Inorg. Chim. Acta 151 (3) (1988) 201–208.
- [20] F.H. Allen, O. Kennard, D.G. Watson, L. Brammer, A.G. Orpen, R. Taylor, Tables of bond lengths determined by X-ray and neutron diffraction. Part 1. Bond lengths in organic compounds, J. Chem. Soc., Perkin Trans. 2 12 (1987) S1–S19.